Supporting Information

Bozoky et al. 10.1073/pnas.1315104110

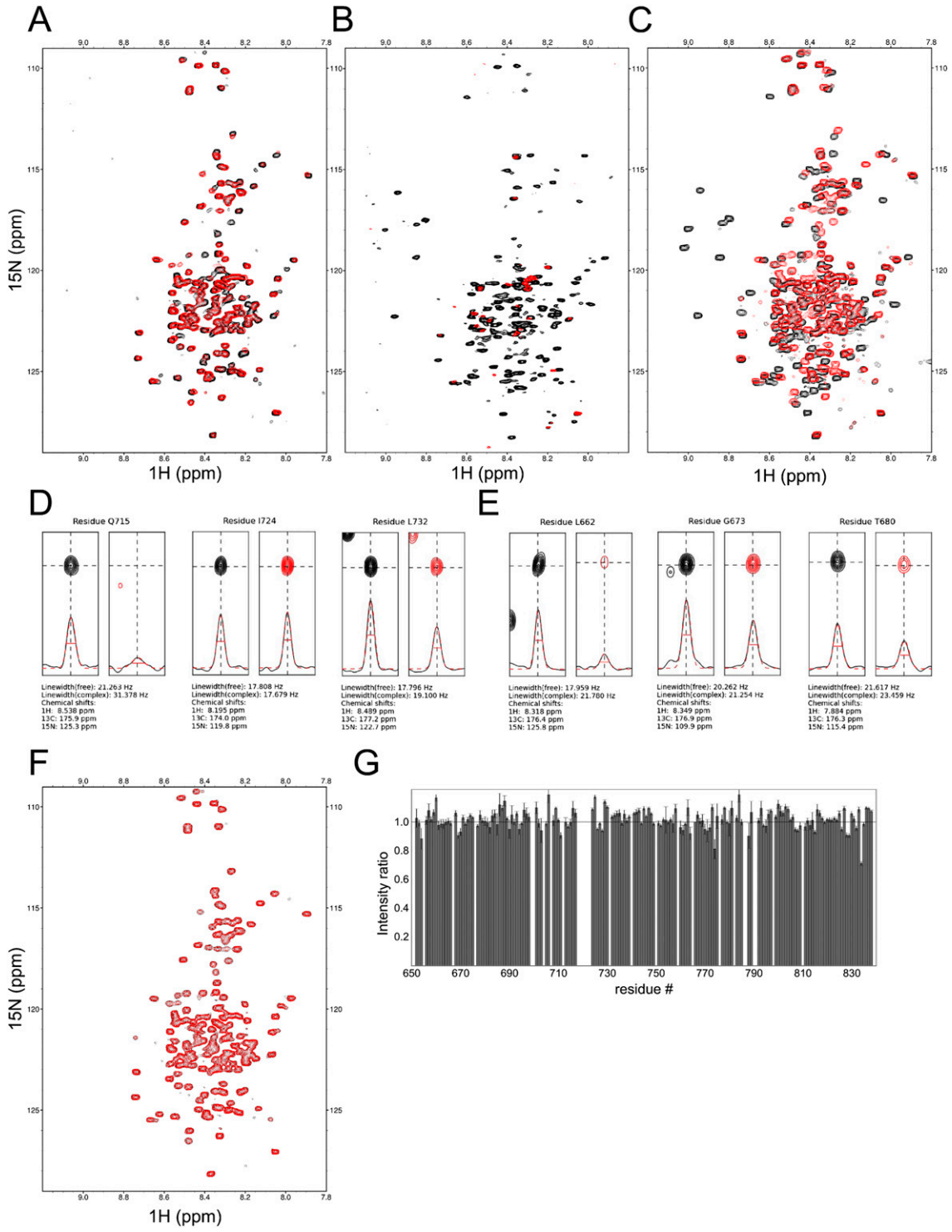

Fig. S1. R region interactions with cystic fibrosis transmembrane conductance regulator (CFTR) nucleotide binding domain 1 (NBD1) and 14-3-3 under near saturating conditions (98% and 99.9%, respectively) and a binding control experiment with ubiquitin. (*A*) NMR HSQC spectra of labeled nonphosphorylated R region in the absence (black) and presence (red) of NBD1. (*B*) HSQC spectra of the PKA-phosphorylated labeled R region in the absence (black) and presence (red) of unlabeled 14-3-3β. To achieve high saturation levels, low R region protein concentration was used. (*C*) Reference HSQC spectra of labeled

Legend continued on following page

nonphosphorylated (red) and PKA-phosphorylated (black) R region. (*D* and *E*) Changes in line shape on binding of (*D*) NBD1 (with nonphosphorylated R region) and (*E*) 14-3-3β (with PKA-phosphorylated R region) for selected resonances of R region. Peaks are showed in the proton–nitrogen dimension of HNCO. Line shapes in proton dimension were fitted (red dashed line) with a Gaussian curve to calculate line widths. Analysis of the changes in line shape on binding clearly shows that resonances with lower intensities on binding are broadened and that resonances with higher intensities are narrowed. Thus, the intensity ratios plotted in the binding profiles provide a measure of broadening effects, likely caused by chemical exchange. (*F*) NMR HSQC spectra of labeled nonphosphorylated R region in the absence (black) and presence (red) of human ubiquitin, with the lack of perturbation indicating no binding. (*G*) Peak intensity ratios (Fig. 1) for nonphosphorylated R region for human ubiquitin showing no interaction.

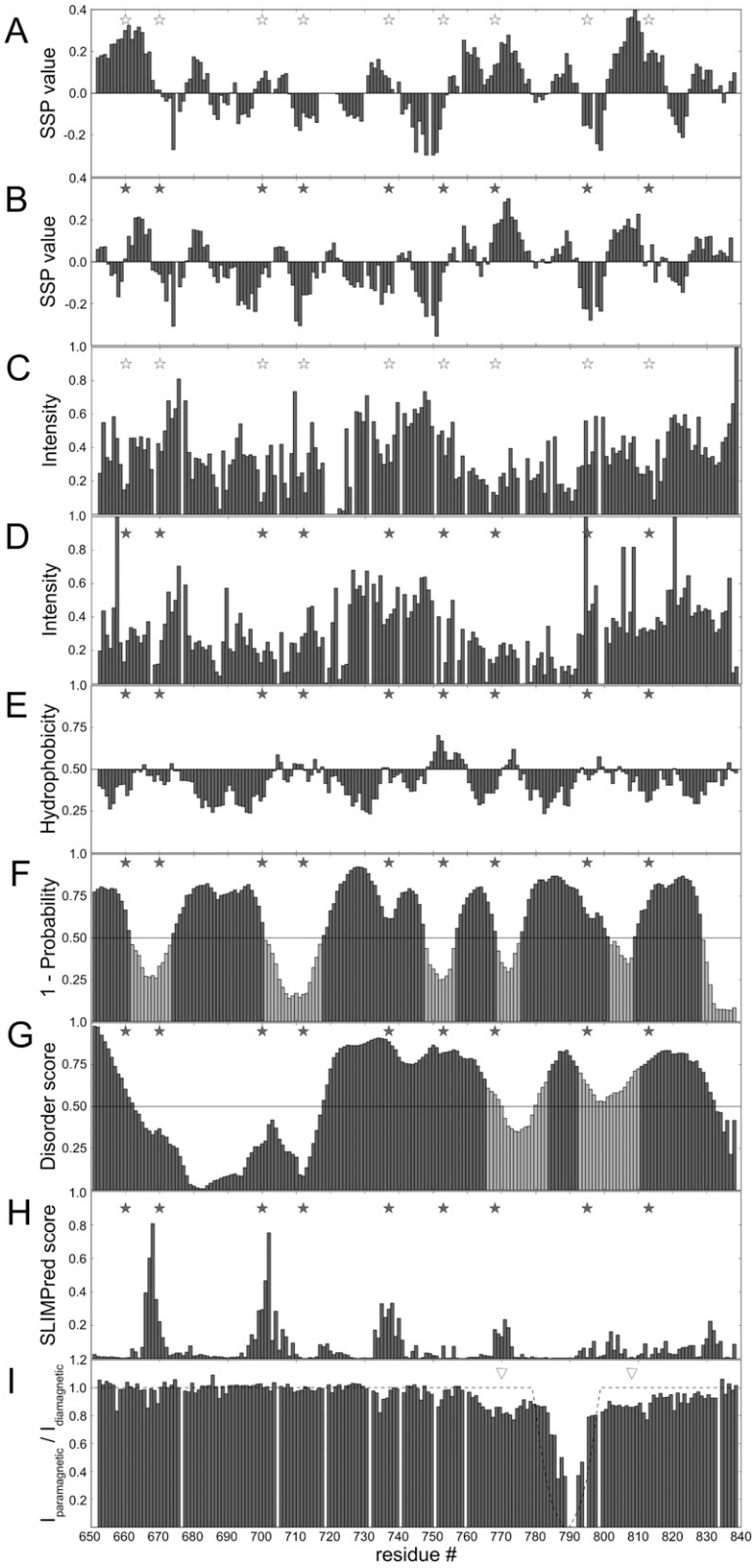

Fig. S2. R region structural data and binding site predictions. (*A* and *B*) Secondary structure propensity (SSP) (1) determination of fractional population of α-helical (positive) and β-structure (negative) conformations based on experimental chemical shifts (2) for (*A*) nonphosphorylated and (*B*) phosphorylated R regions of human CFTR. (*C* and *D*) R region peak intensities for (*C*) nonphosphorylated and (*D*) PKA-phosphorylated free states normalized to the highest intensities in each spectrum. Intensity variation is likely caused by fluctuating intramolecular secondary structure and tertiary contacts. (*E*) Hydrophobicity plot of the regulatory region based on the hydropathy index (http://web.expasy.org/cgi-bin/protscale/protscale.pl). Values higher than 0.5 reflect hydrophobic regions and lower values show hydrophilic regions using a 9-residue-wide averaging window and a linear weighting model. (*F*) Binding segment prediction

Legend continued on following page

using the ANCHOR binding region predictor (3) for disordered proteins. One minus probability is plotted to be consistent with other predictions and measured binding data. Values lower than 0.5 indicate a binding segment (plotted as lighter gray). (*G*) Disorder prediction using PONDR VL-XT (4–6). Lighter color represents the predicted binding regions by Alpha-MoRFpredII (7). (*H*) SLiMPred prediction (8). Higher values represent higher probability of a linear motif binding target. Phosphorylation sites of the cAMP-dependent protein kinase are marked as stars (open for the nonphosphorylated and gray for the phosphorylated states for experimental data in *A–D*; gray for the calculated and predicted values in *E–H*). (*I*) Paramagnetic relaxation enhancement data for nonphosphorylated, S-(2,2,5,5-tetramethyl-2,5-dihydro-1H-pyrrol-3-yl)methyl methanesulfonothioate (MTSL)-labeled R region mutant A789C/C833S represented as the intensity ratios ($I_{paramagnetic}/I_{diamagnetic}$). The dashed line gives the expected values caused by the MTSL labeling for a random coil chain. Residue 789 shows nonrandom contacts with residues around 770 and 808, which are sites of NBD1 interactions (indicated with triangles).

1. Marsh JA, Singh VK, Jia Z, Forman-Kay JD (2006) Sensitivity of secondary structure propensities to sequence differences between alpha- and gamma-synuclein: Implications for fibrillation. *Prot Sci* 15(12):2795–2804.
2. Baker JMR, et al. (2007) CFTR regulatory region interacts with NBD1 predominantly via multiple transient helices. *Nat Struct Mol Biol* 14(8):738–745.
3. Dosztányi Z, Mészáros B, Simon I (2009) ANCHOR: Web server for predicting protein binding regions in disordered proteins. *Bioinformatics* 25(20):2745–2746.
4. Li X, Romero P, Rani M, Dunker AK (1999) Predicting protein disorder for N-, C-, and internal regions. *Genome Inform* 10:30–40.
5. Romero P, et al. (2001) Sequence complexity of disordered protein. *Proteins* 42(1):38–48.
6. Romero P, Obradovic Z, Dunker AK (1997) Sequence data analysis for long disordered regions prediction in the calcineurin family. *Genome Inform* 8:110–124.
7. Cheng, Y, et al. (2007) Mining alpha-helix-forming molecular recognition features with cross species sequence alignments. *Biochemistry* 46(47):13468–13477.
8. Davey NE, Haslam NJ, Shields DC, Edwards RJ (2010) SLiMFinder: A web server to find novel, significantly over-represented, short protein motifs. *Nucl Acids Res* 38(suppl 2):W534-W539.

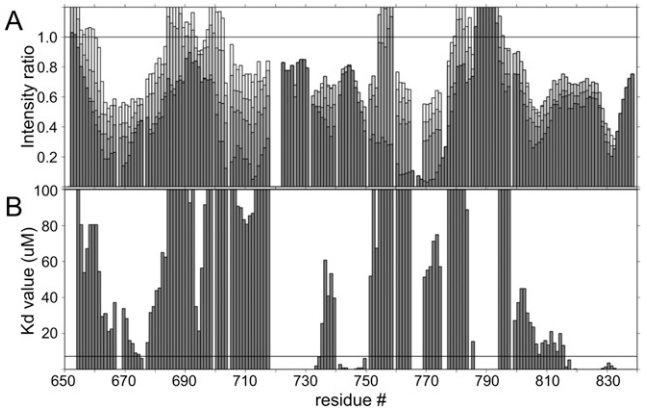

Fig. S3. Residue-specific binding constant calculations for the interaction of R region with NBD1 based on peak broadening. (*A*) Nonphosphorylated R region binding profiles on binding to increasing amounts of NBD1 (white to black; corresponds to 1:1, 1:2, 1:3, and 1:8 molar ratios of R region:NBD1). (*B*) K_d values calculated using a single site model fitting five data points from titration experiments with 1:0, 1:1, 1:2, 1:3, and 1:8 molar ratios (R region:NBD1). Solid line represents the value 7.1 μM, the macroscopic binding constant determined from fluorescence titrations. Although the quantitative interpretation of broadening as a measure of residue-specific binding is complicated by the convolution of effects caused by τ_c and chemical exchange within the bound state, the trends observed are consistent with the model of multiple interacting segments having different local affinities for NBD1.

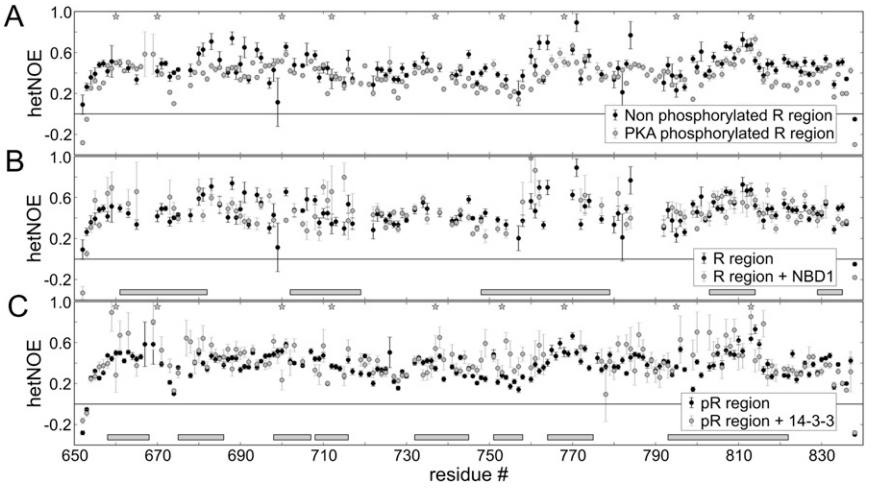

Fig. S4. Heteronuclear ^{1}H-^{15}N NOE experiments (hetNOE). (*A*) Nonphosphorylated (black) and PKA-phosphorylated (gray) R region NOE values. (*B*) Nonphosphorylated R region NOE values in the absence (black) and presence (gray) of NBD1 (97.5% saturation of binding). (*C*) PKA-phosphorylated R (pR) region NOE values in the absence (black) and presence (gray) of 14-3-3β (98.3% saturation of binding). Gray bars indicate (*B*) the interacting segments of the nonphosphorylated R region on binding to NBD1 or (*C*) the phosphorylated R region on binding to 14-3-3β derived from HNCO experiments. PKA phosphorylation sites are marked as stars. Error bars are calculated based on the error propagation of NMR data.

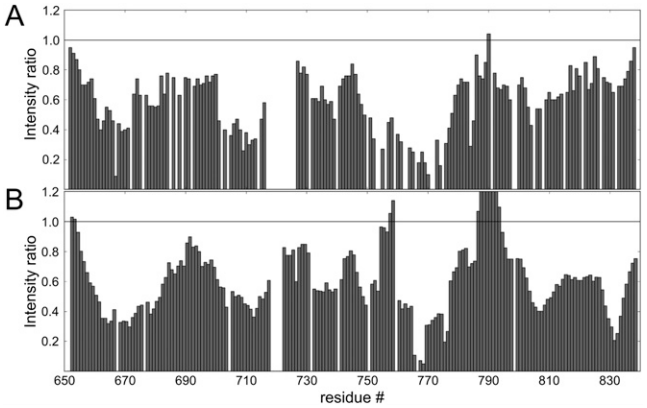

Fig. S5. R region binding profiles on addition of mouse and human NBD1. Peak intensity ratios in the presence and absence of binding partner (Fig. 1) for the nonphosphorylated R region with (*A*) mouse (1) and (*B*) human NBD1 from experiments with the closest matched concentrations [R region concentrations (*A*) 50 and (*B*) 150 μM and 1:2 NBD1:R region molar ratio]. Solid lines represent the value one, the baseline expectation for no binding with no intensity change observed. Sequence differences between mouse and human NBD1 and, most notably, the presence of the regulatory insertion in the mouse NBD1 construct used give rise to slightly different resulting patterns in the binding profiles.

1. Baker JMR, et al. (2007) CFTR regulatory region interacts with NBD1 predominantly via multiple transient helices. *Nat Struct Mol Biol* 14(8):738–745.

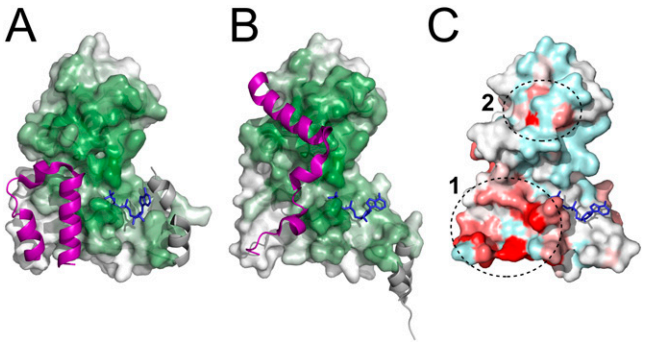

Fig. S6. Comparison of R region:NBD1 interaction. Surface representation of the (*A*) mouse NBD1 X-ray structure [Protein Data Bank (PDB) ID code 1R0X] and (*B*) human NBD1 X-ray structure (PDB ID code 1XMI) oriented to show the NBD2 perspective. The N terminus of R region (aa 638–671) is colored in purple. Surface representation is colored as a green gradient reflecting proximity to atoms in the other NBD1 molecule within the NBD1:NBD1 homodimer structure (PDB ID code 2PZE). Flexible residues of the regulatory insertion of NBD1 (aa 405–437) are displayed in gray ribbon representation only. (*C*) NBD1 resonance intensity reductions on binding to R region (PDB ID code 2PZE) as shown in Fig. 3. Coloring is the same as used in Fig. 3.

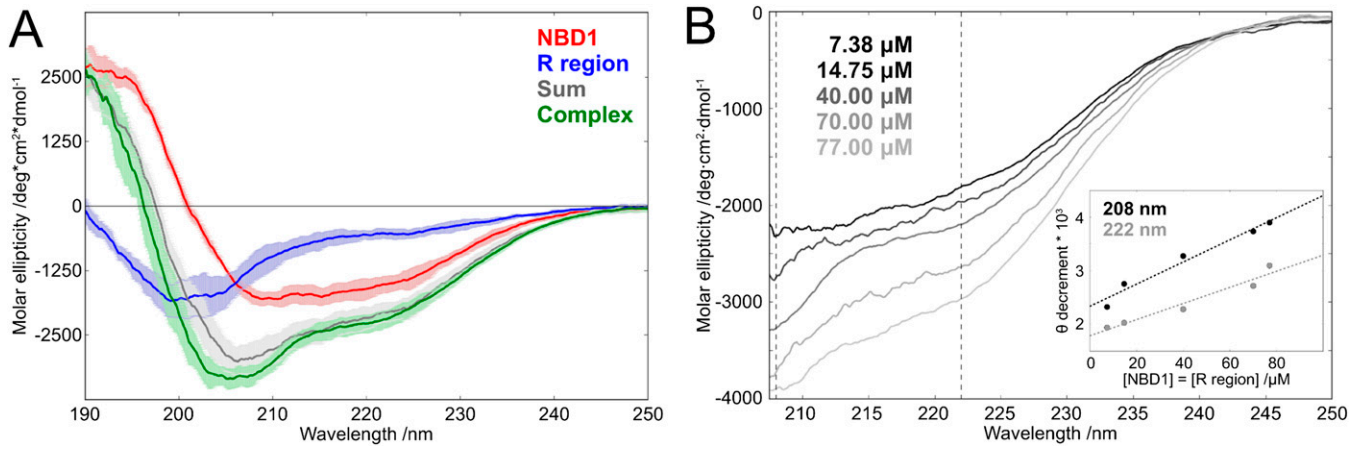

Fig. S7. CD measurements on the nonphosphorylated R region:NBD1 complex. (*A*) CD curve of NBD1 (red), R region (blue), the sum of the NBD1 and R region curves (gray), and a 1:1 complex (green) at 40 μM concentration. Error bars represent 1 SD calculated from five parallels with three repeats each. (*B*) Molar ellipticity of 1:1 complex at different concentrations (7.38, 14.75, 40.0, 70.0, and 77.0, respectively). Wavelengths 208 and 222 nm are marked with dashed lines, and the values are presented in *Inset* (black, 208; gray, 222). At higher concentration, the complex formation is increased (saturation levels: 38%, 51%, 66%, 73%, and 74%, respectively) along with the complex contribution to the CD curve.

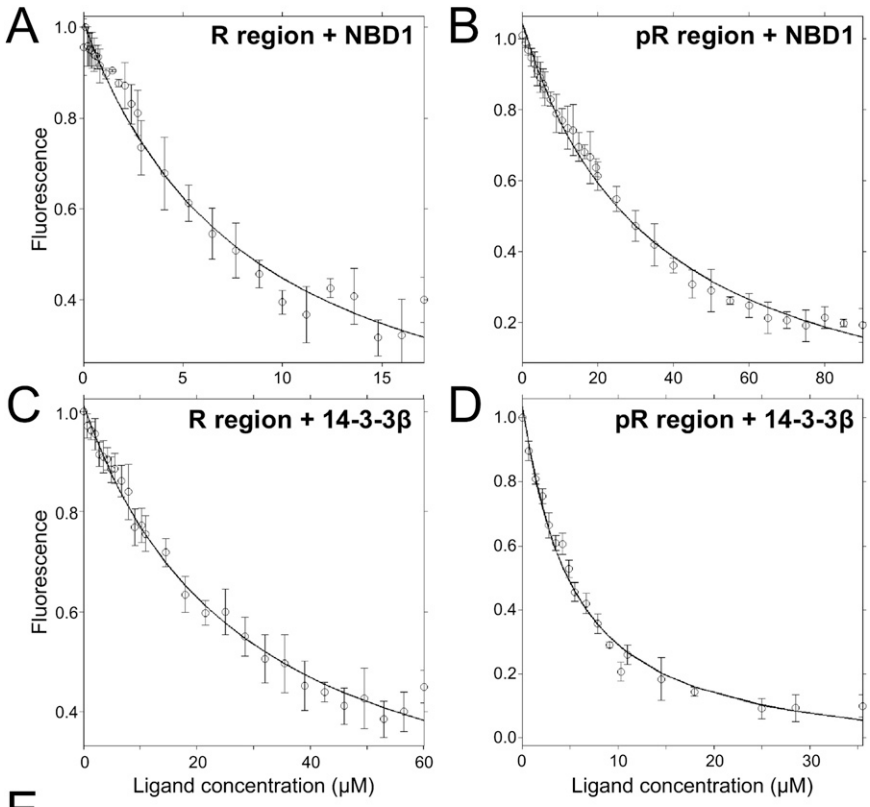

E

Partners	Kd	$\chi 2$
R + NBD1	7.1 ± 2.8 μM	$3.0 \cdot 10^{-2}$
pR + NBD1	28.9 ± 3.4 μM	$9.4 \cdot 10^{-3}$
R + 14-3-3β	34.3 ± 7.4 μM	$3.5 \cdot 10^{-4}$
pR + 14-3-3β	5.4 ± 1.0 μM	$1.6 \cdot 10^{-3}$

Fig. S8. Fluorescence binding curves for titration of human NBD1 with (*A*) nonphosphorylated R region and (*B*) PKA-phosphorylated R region (pR) and titration of human 14-3-3β with (*C*) nonphosphorylated R region and (*D*) pR. Solid lines represent the fitted curves to the tryptophan fluorescence changes with a single site binding model. (*E*) Summary table of the binding constants. Tryptophan probes are located at residues 401 and 496 of NBD1 and residues 61 and 230 of 14-3-3β.

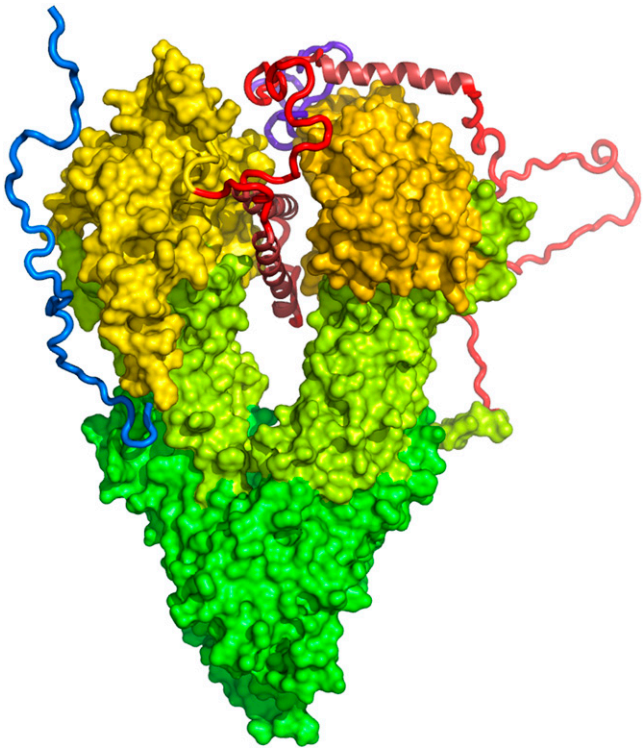

Movie S1. Animated structural model of full-length CFTR in the nonphosphorylated R region state representing a closed channel state and showing 10 selected conformers using the same color scheme as used in Fig. 5.

Movie S1